Catalysts **2012**, *2*, 1-23; doi:10.3390/catal2010001

OPEN ACCESS

catalysts

ISSN 2073-4344

www.mdpi.com/journal/catalysts

Article

Gold/Iron Carbonyl Clusters for Tailored Au/FeO_x Supported Catalysts

Rosa Bonelli [1], Stefano Zacchini [2] and Stefania Albonetti [1,*]

[1] Dipartimento di Chimica Industriale e dei Materiali, Università di Bologna, Viale Risorgimento 4, Bologna 40136, Italy; E-Mail: rosa.bonelli@unibo.it

[2] Dipartimento di Chimica Fisica ed Inorganica, Università di Bologna, Viale Risorgimento 4, Bologna 40136, Italy; E-Mail: stefano.zacchini@unibo.it

* Author to whom correspondence should be addressed; E-Mail: stefania.albonetti@unibo.it.

Received: 6 October 2011; in revised form: 1 December 2011 / Accepted: 6 December 2011 / Published: 21 December 2011

Abstract: A novel preparation method was developed for the preparation of gold/iron oxide supported catalysts using the bimetallic carbonyl cluster salts $[NEt_4]_4[Au_4Fe_4(CO)_{16}]$ and $[NEt_4][AuFe_4(CO)_{16}]$ as precursors of highly dispersed nanoparticles over different supports. A series of catalysts with different metal loadings were prepared and tested in the complete oxidation of dichlorobenzene, toluene, methanol and in the preferential oxidation of CO in the presence of H_2 (PROX) as model reactions. The characterization by BET, XRD, TEM, H_2-TPR, ICP-AES and XPS point out the way the nature of the precursors and the thermal treatment conditions affected the dispersion of the active phase and their catalytic activity in the studied reactions.

Keywords: cluster derived catalysts; gold/iron catalysts; catalytic combustion

1. Introduction

In recent years we have witnessed an exponential growth in scientific discoveries concerning catalysis by gold, and numerous applications have been found for Au-based catalysts [1,2]. The literature contains several studies on the use of gold-based catalysts for environmental applications, and good results are reported for the catalytic combustion of different volatile organic compounds (VOCs) [3–6]. Moreover, recently it has also been established that gold-based catalysts are potentially

capable of being effectively employed in fuel cells in order to remove CO traces by preferential CO oxidation in H_2-rich streams [7].

Catalytic materials incorporating bimetallic particles dispersed on high-surface-area supports have attracted increasing attention because of their properties, which are markedly different from either of the constituent metals, and above all for their enhanced catalytic activity, selectivity and stability [8–10]. Regarding gold based catalysts, in the literature there are several studies demonstrating the beneficial effect of the addition of a second metal to the active phase [11–14]. In particular, the addition of iron component to gold catalysts was reported to lead to improved systems in terms of enhanced activity, selectivity, resistance to deactivation, and prolonged lifetime of the catalyst [15,16]. The catalytic behavior of Au in these catalysts is significantly affected by the presence of the Fe. For example, FeO_x species were found to act as a structural promoter but also as a co-catalyst: it was proved that in the presence of FeO_x, gold particles were stabilized against sintering, while the lattice oxygen of the oxide plays an active role via the Mars-van Krevelen mechanism [17]. Corma *et al*. demonstrated that the addition of iron to gold supported on high-surface-area TiO_2 leads to an increased number of oxygen defect sites and then to enhanced oxygen activation on this kind of sites, which generate oxygen vacancies [15]. Recent studies [18,19] have shown that $Au/FeO_x/CeO_2$ catalysts are very active for total and preferential CO oxidation. Improved catalytic performance has been related to the synergy between gold-cerium-iron and the enhanced reducibility due to the strong interaction of ceria with iron and gold, the latter being facilitated by iron. In fact, the presence of iron in the CeO_2 structure was found to increase Au dispersion by creating sites with an increased electronic density, which act in a similar way to oxygen vacancies. The deposition of gold nanoparticles is facilitated at these sites.

Since the catalytic behavior of multi-component supported catalysts is strongly affected by the size of the metal particles and by their reciprocal interaction, the method of synthesis plays a crucial role in obtaining active bimetallic nanoparticles with controlled dimensions and a uniform composition. The use of bimetallic cluster complexes, with a nanometric size and a well-defined molecular structure, as catalyst precursors has recently attracted attention as a viable method for preparing new stoichiometrically-precise bimetallic nanocatalysts [20] in which both the pristine vicinity and the interaction between the metal components could be retained in the final material. Among these, metal carbonyl clusters are quite attractive candidates, as they decompose under very mild conditions [21–23]. The chemistry of these clusters is extremely well established at the molecular level, in terms of their synthesis and their chemical, physical and structural properties. In addition, species with different sizes and compositions can be prepared [24]; nevertheless, before our study, no such clusters were used for the preparation of supported Au/Fe catalysts.

Following the above considerations, in this paper we report a summary of our ongoing study on the preparation, characterization, and catalytic activity of cluster-derived Au/FeO_x catalysts.

2. Results and Discussion

2.1. Interaction of Carbonyl Clusters with Different Supports

The impregnation processes with the cluster solutions of $[NEt_4]_4[Au_4Fe_4(CO)_{16}]$, $[NEt_4][AuFe_4(CO)_{16}]$ and $[NEt_4][HFe_3(CO)_{11}]$ on the different oxidic supports examined, *i.e.*, TiO_2, CeO_2 and SBA-15, have

been monitored via FTIR in order to better understand these processes and the different phenomena occurring during impregnation. The general procedure followed was: (i) to suspend and stir the support in acetone under nitrogen; (ii) to slowly add to it an acetone solution containing the appropriate amount of cluster; (iii) to stir the mixture overnight under nitrogen; (iv) to remove the solvent in vacuum. The dried powders were then thermally treated as described in the next section. FTIR spectra were recorded (1) on the starting acetone solution of the cluster, (2) on the acetone solution after being in contact overnight with the support, (3) on the dried powder in a nujol mull, and (4) after extraction from the dried powder with CH_3CN. Acetonitrile was used instead of acetone in the last stage because of its greater capability to solubilize these metal clusters.

In the case of TiO_2 as the support, FTIR studies (Figure 1a,b) showed that $[NEt_4][AuFe_4(CO)_{16}]$ and $[NEt_4][HFe_3(CO)_{11}]$ are adsorbed without the occurrence of any reaction, whereas significant changes have been observed during the adsorption of $[NEt_4]_4[Au_4Fe_4(CO)_{16}]$ (Figure 1c).

Figure 1. FTIR spectra in the ν(CO) region obtained during catalyst preparation: (**a**) $[NEt_4][AuFe_4(CO)_{16}]$; (**b**) $[NEt_4][HFe_3(CO)_{11}]$; (**c**) $[NEt_4]_4[Au_4Fe_4(CO)_{16}]$; (1) starting acetone solution of the cluster; (2) acetone solution after being in contact overnight with the support; (3) in vacuum dried powder; (4) CH_3CN extraction from the dried powder; (5) sample after thermal treatment in air.

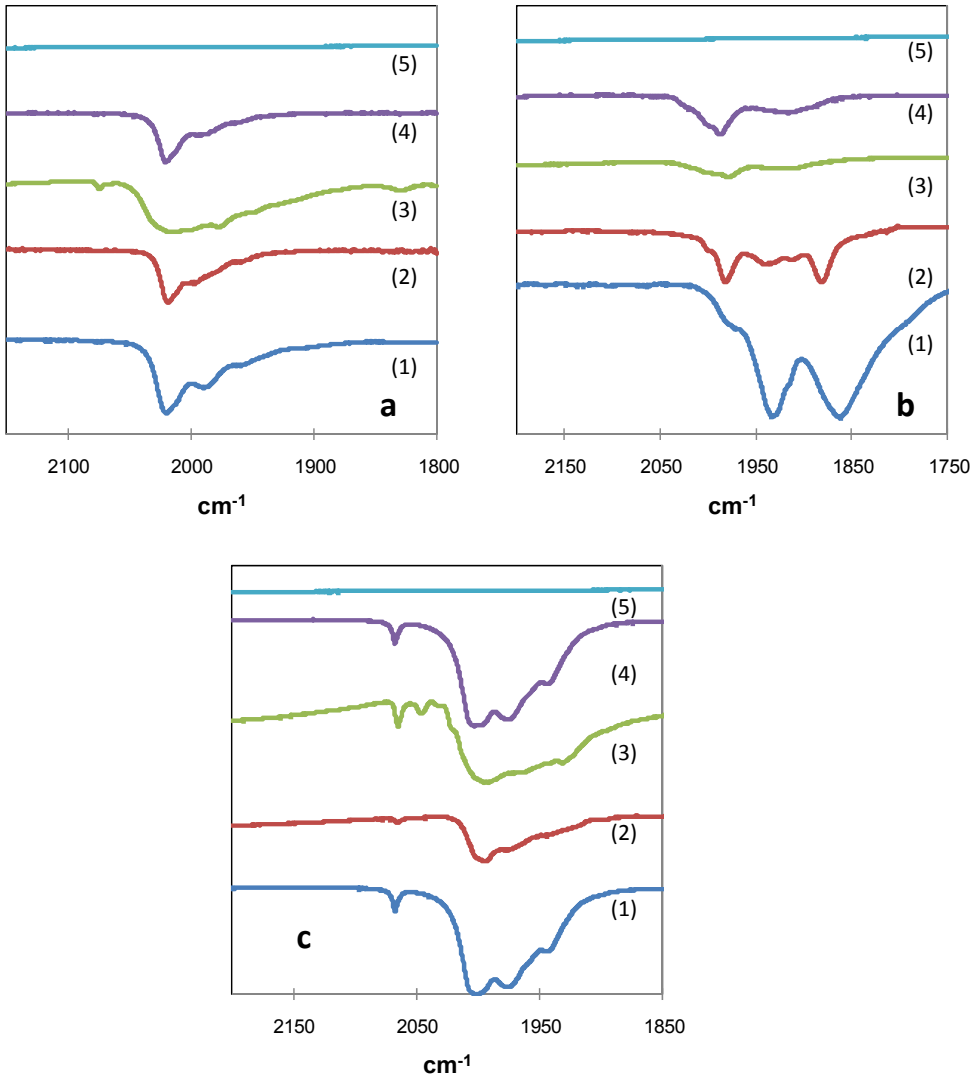

For all systems, the carbonyl cluster is totally decomposed after thermal treatment, since no ν(CO) band is present in the final spectra. It is clear that the two bimetallic clusters not only have a different Au:Fe composition, but also a rather different chemical behavior. Thus, whereas $[NEt_4][AuFe_4(CO)_{16}]$ is quite stable and non-reactive, $[NEt_4]_4[Au_4Fe_4(CO)_{16}]$ is very reactive, being easily oxidized as indicated by the increased ν(CO), yielding other Au-Fe carbonyl species. Moreover, the final product of its oxidation is $[NEt_4][AuFe_4(CO)_{16}]$.

Several other Au-Fe carbonyl species exist between these two species and, among these, $[Au_5Fe_4(CO)_{16}]^{3-}$ [ν(CO) 1945(s) and 1861 (s) cm^{-1}], $[Au_{21}Fe_{10}(CO)_{40}]^{6-}$ [ν(CO) 1982 (s), 1937 (sh), 1889 (sh) cm^{-1}], $[Au_{22}Fe_{12}(CO)_{48}]^{6-}$ [ν(CO) 1980 (s), 1925 (sh), 1880 (sh) cm^{-1}], $[Au_{28}Fe_{14}(CO)_{52}]^{8-}$ [ν(CO) 1985 (s), 1927 (sh), 1887 (sh) cm^{-1}], and $[Au_{34}Fe_{14}(CO)_{50}]^{10-}$ [ν(CO) 1990 (s), 1932 (sh), 1900 (sh) cm^{-1}] have been recently structurally characterized [25,26]. Overall, these brown species are intermediates in the oxidation in solution of $[Au_4Fe_4(CO)_{16}]^{4-}$ to eventually give $[AuFe_4(CO)_{16}]^-$. All this information can be helpful for fully understanding the fate of $[Au_4Fe_4(CO)_{16}]^{4-}$ during impregnation on TiO_2.

FTIR studies indicate that the oxidation of $[Au_4Fe_4(CO)_{16}]^{4-}$ occurs in two different steps during catalyst preparation, as can be inferred from Figure 1c, showing the comparison of the FTIR spectra in the ν(CO) region of: (1) $[NEt_4]_4[Au_4Fe_4(CO)_{16}]$ in acetone [ν(CO) 1931 (s) and 1861 (s) cm^{-1}]; (2) the acetone solution after being in contact with TiO_2 [ν(CO) 1982 (s) 1940 (m), 1913(w) and 1881 (s) cm^{-1}]; (3) the powder (in nujol mull) after removal in vacuum of the solvent [ν(CO) 2000 (sh) 1978 (s) and 1917(m) cm^{-1}]; (4) the CH_3CN extraction from the dried powder [ν(CO) 2000 (sh) 1986 (s) and 1914 (m) cm^{-1}] (nominal composition of the powder 4 wt.% Au).

Similar experiments have been carried out with different cluster loadings, showing the dependence of oxidation on the cluster: TiO_2 ratio.

As soon as the acetone solution of $[Au_4Fe_4(CO)_{16}]^{4-}$ comes into contact with TiO_2, the cluster reacts, resulting in more oxidized species such as $[Au_5Fe_4(CO)_{16}]^{3-}$ or mixtures of the above-mentioned brown compounds, depending on the cluster: TiO_2 ratio; the more cluster is added, the less oxidation is observed. The latter species contain an Au:Fe ratio higher than the precursor $[Au_4Fe_4(CO)_{16}]^{4-}$ and the excess Fe is released in the form of $[HFe(CO)_4]^-$ as indicated by ν(CO) at 1,881 cm^{-1}. The oxidant is likely to be TiO_2 and, therefore, Ti(IV) is partially reduced, as indicated by the fact that the solid turns from white to grey. This is also in agreement with the fact that the degree of oxidation of the cluster increases by increasing the amount of TiO_2 (lower Au wt.%). Further reaction then occurs when the clusters are forced into closer contact with TiO_2 by removal of the solvent in a vacuum, as indicated by the changes in the FTIR spectra.

The carbonyl species present at this point on the solid support can be extracted with a polar solvent such as CH_3CN, and this makes it easier to compare their FTIR features with the ones reported for the Au-Fe clusters studied in solution. This analysis confirms that the species formed on the solid support at the end of the deposition process are oxidized clusters such as brown $[Au_{21}Fe_{10}(CO)_{40}]^{6-}$, $[Au_{22}Fe_{12}(CO)_{48}]^{6-}$, $[Au_{28}Fe_{14}(CO)_{52}]^{8-}$, $[Au_{34}Fe_{14}(CO)_{50}]^{10-}$, and green $[AuFe_4(CO)_{16}]^-$. The brown species are favored by a high load of cluster (4–6 wt.%), whereas the latter increases by lowering the amount of cluster (1–2 wt.%). Oxidation of $[HFe(CO)_4]^-$ is observed, also, yielding mainly $[HFe_3(CO)_{11}]^-$ [ν(CO) 2000 (s) cm^{-1}], as also confirmed by independent experiments where $[HFe(CO)_4]^-$ has been directly deposited on TiO_2 following the same procedure.

On the contrary, it was observed that no chemical reaction occurs during any phase of the impregnation process of $[NEt_4][AuFe_4(CO)_{16}]$ on TiO_2 (Figure 1a). This salt displays a strong ν(CO) band in acetone at 2018 cm^{-1}, which is also maintained after adsorption on TiO_2 both in solution and in the solid state. Moreover, the intact starting cluster can be recovered from the solid by extraction with CH_3CN. These results are independent from the cluster loading.

Nevertheless, a careful inspection of the FTIR spectra of supported $[NEt_4][AuFe_4(CO)_{16}]$ before thermal decomposition, in addition to minor changes on the terminal ν(CO) region, indicates the presence in the solid state of edge-bridging carbonyls with typical ν(CO) at 1826 and 1778 cm^{-1}, which are negligible in CH_3CN solution. This difference be accounted for by the following equilibrium (1) between the two structural isomers $[AuFe_4(CO)_{16}]^-$ (all terminal CO) and $[AuFe_4(CO)_{14}(\mu\text{-}CO)_2]^-$ (two bridging CO).

$$[AuFe_4(CO)_{16}]^- \rightleftharpoons [AuFe_4(CO)_{14}(\mu\text{-}CO)_2]^- \quad (1)$$

Both these isomers were structurally characterized, and an equilibrium constant $K \sim 10^{-2}$ in solution was established [27]. In the present case, interaction with the TiO_2 support likely shifts the equilibrium toward the $[AuFe_4(CO)_{14}(\mu\text{-}CO)_2]^-$ isomer after deposition.

FTIR investigation was also carried out during preparation of the Fe-TiO_2 catalysts employing $[NEt_4][HFe_3(CO)_{11}]$ as precursor, showing the occurrence of no reaction.

Very similar results were obtained on CeO_2 and SBA-15, and therefore they will not be discussed any further.

2.2. Effect of Catalyst Thermal Treatment

Cluster decomposition was investigated by thermal analyses in order to better understand how this process can be influenced by temperature and atmosphere composition. Then the conditions for the thermal treatment of the samples were optimized in order to set the parameters and basically avoid or minimize Au sintering. In order to verify the cluster decomposition processes and then understand what the best conditions for catalyst thermal treatment are, a thermal study was carried out on bulk clusters by means of TGA and DSC analyses. The information obtained, on the extent of the weight losses and the temperatures at which they occur, can be useful in understanding (i) how the clusters decompose due to the effect of the temperature and (ii) what products arise from their decomposition. Performing the analyses in air and in nitrogen also helps understand the effect of the atmosphere composition. The TGA analyses of $[NEt_4][HFe_3(CO)_{11}]$ (Figure 2a) show that the decomposition process seems to take place in a single step in air, while two different processes can be distinguished under nitrogen. In both cases the results agree with quantitative formation of iron oxides.

XRD analyses on bulk samples decomposed under similar experimental conditions indicate Fe_3O_4 as the more likely product. Nevertheless, for this cluster salt, the temperature at which a constant weight is reached depends on whether the TGA is performed in air (approximate 60 °C) or under nitrogen (approximate 275 °C). It is well known, in fact, that when iron is in a very disperse form, as in this case, it is highly pyrophoric; then the decomposition/oxidation of the iron carbonyl cluster in air is very fast. Thus, the combustion of the iron cluster salt in air seems to be more efficient than its thermal decomposition under nitrogen.

Figure 2. TGA analyses of bulk cluster samples: (**a**) $[NEt_4][HFe_3(CO)_{11}]$; (**b**) $[NEt_4]_4[Au_4Fe_4(CO)_{16}]$; (**c**) $[NEt_4][AuFe_4(CO)_{16}]$. (—) in air and (—) under nitrogen.

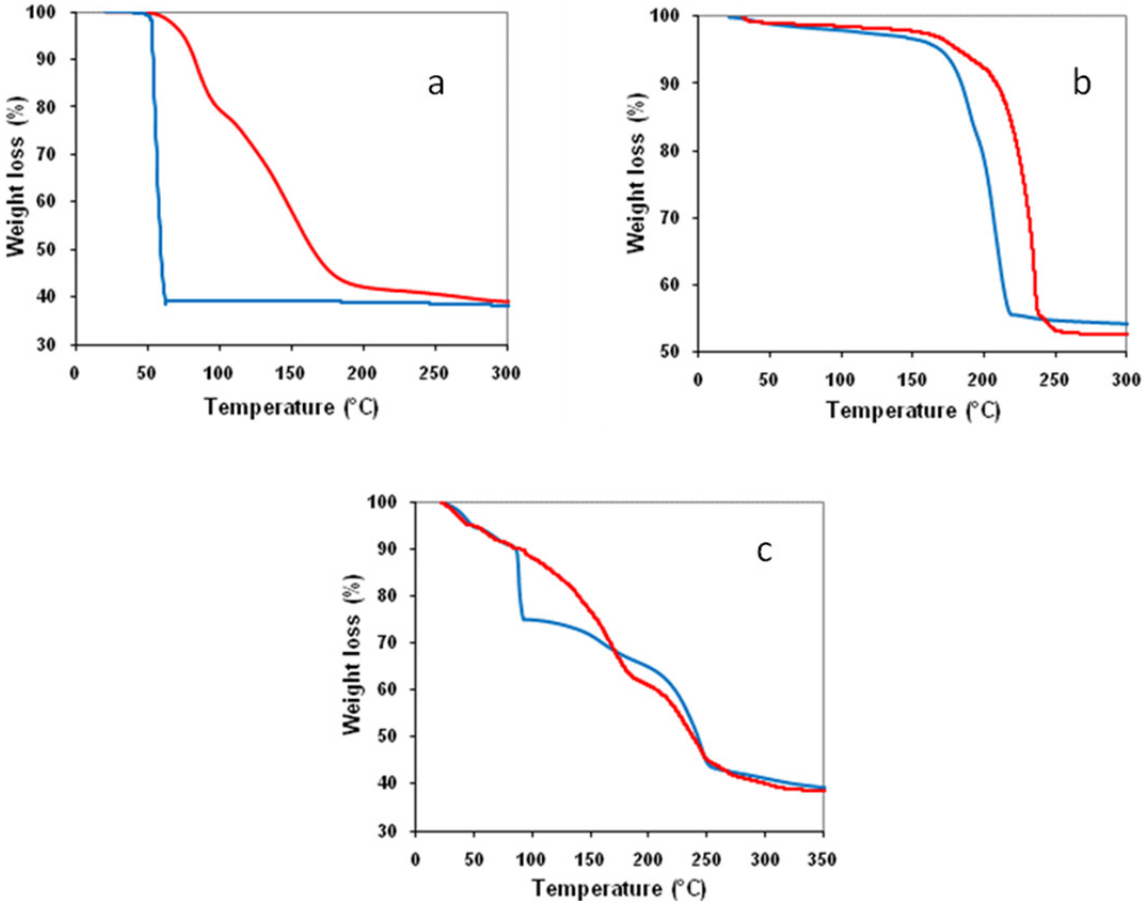

The same analyses were performed for the bi-metallic cluster $[NEt_4]_4[Au_4Fe_4(CO)_{16}]$. In Figure 2b it can be seen how the weight loss is similar in air and under nitrogen, and the decomposition occurs at approx. 150 °C in a single step. In this case, the final weight is 55% of the initial one; this value is lower than expected if the bi-metallic cluster decomposes to Au + Fe_2O_3 (67%) or Au + Fe_3O_4 (66%). Since it is extremely unlikely that the observed discrepancy is due to a gold loss from the bulk, probably some iron is lost in the form of the volatile $Fe(CO)_5$.

Different results have been obtained for $[NEt_4][AuFe_4(CO)_{16}]$ decomposition (Figure 2c). Indeed, for this cluster the molar ratio Fe/Au is higher than in $[NEt_4]_4[Au_4Fe_4(CO)_{16}]$ and the oxidation state of Au is different; both these factors influence the reactivity of the cluster and its decomposition. The samples in air as well as under nitrogen reach a constant weight, which is approx. 35% of the starting one be lost in order to justify the final weight.

Regarding the TGA profile obtained in air, it is rather likely that the first process occurring at approx. 100 °C is the decarbonylation of the cluster, followed by the thermal combustion of the organic cation and iron oxidation.

Calorimetric data reported in Figure 3 confirmed this hypothesis, indicating that a strong exothermic phenomenon occurs in air at temperatures higher than 120 °C, while only rather feeble endothermic processes occur under nitrogen at ~100 °C, 150 °C and 200 °C.

Figure 3. DSC analyses of bulk $[NEt_4][AuFe_4(CO)_{16}]$ (—) in air and (—) under nitrogen.

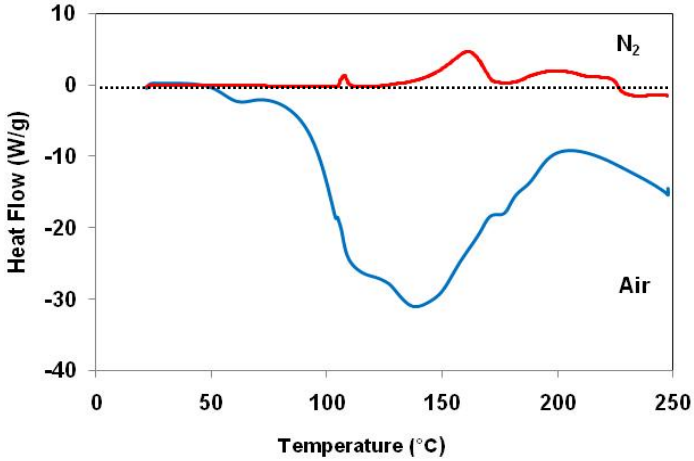

In order to optimize thermal treatment conditions for bi-metallic catalysts, a $Fe_{0.6}Au_2$-Ti sample was thermally treated at 400 °C in three different gas atmospheres: air, nitrogen and hydrogen.

Au crystallites, as determined from XRD line broadening, were found to significantly sinter during calcination in air (Figure 4), but did not greatly change after thermal treatment under N_2 and H_2.

Figure 4. Effect of the thermal treatment conditions on Au particles size for $Fe_{0.6}Au_2$-Ti sample.

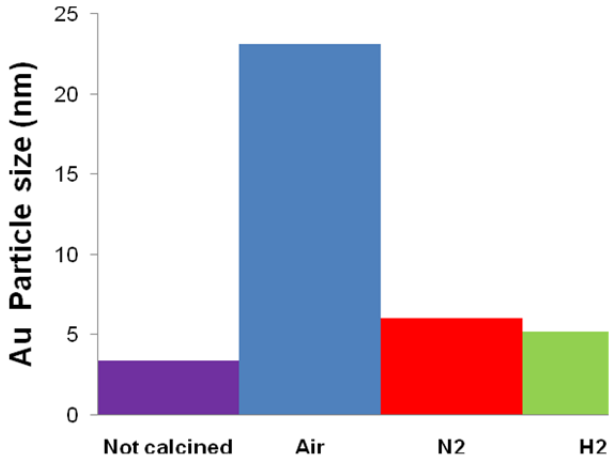

These results indicate an appreciable agglomeration of gold particles upon calcination in air, confirming the hypothesis that the cluster transformation in the presence of an oxidizing atmosphere could lead to uncontrolled decomposition with rapid temperature rise, causing gold nanoparticles sintering, but underscore the possibility of directing the size of gold particles by controlling cluster oxidation/decomposition. Thus the supported bi-metallic catalysts were thermally treated under nitrogen while the iron catalysts were calcined in air, because the performances of the latter materials are not affected by a similar treatment [28].

The effect of the thermal treatment temperature on Au/FeO_x-Ce performances was also investigated. In this case the $Fe_{2.3}Au_2$-Ce sample was prepared as usual, but after drying in air ($Fe_{2.3}Au_2$-Ce-D sample), one part of the sample was treated under nitrogen at 200 °C ($Fe_{2.3}Au_2$-Ce-D-200 sample), while the other part was characterized and used as is. These two samples were then compared with $Fe_{2.3}Au_2$-Ce thermally treated at 400 °C in nitrogen ($Fe_{2.3}Au_2$-Ce-D-400 sample).

The average size of gold particles, evaluated through the reflection at 2θ 38.2° (Table 1), indicated the achievement of a higher dispersion by thermally treating the catalyst at 200 °C and 400 °C than with simple drying. Moreover, as also observed for TiO_2 supported samples, raising the temperature to 400 °C under nitrogen does not lead to any detrimental effect on gold particle size.

Table 1. Surface area and Au crystal size for $Fe_{2.3}Au_2$-Ce samples depending on thermal treatment temperature.

Catalyst	Drying conditions	Thermal treatment conditions	Surface Area (m^2/g)	Au particle size (nm)
$Fe_{2.3}Au_2$-Ce-D	Air at 100 °C	-	-	7.7
$Fe_{2.3}Au_2$-Ce-D-200	Air at 100 °C	N_2 at 200 °C	64	4.6
$Fe_{2.3}Au_2$-Ce-D-400	Air at 100 °C	N_2 at 400 °C	73	4.8

A beneficial effect due to the higher thermal treatment temperature in N_2 was also observed on the surface area; this effect was probably due to the fact that at 200 °C the cationic part of the cluster salt (tetra-ethyl ammonium) was only partially decomposed, blocking part of support porosity. In fact, the TGA-DTA in nitrogen of $[NEt_4][AuFe_4(CO)_{16}]$ salt showed a significant weight loss after 200 °C.

Despite the absence of any chemical reaction during cluster salts impregnation on different supports, ICP analysis on the catalysts indicated that the real metal content differs significantly from the nominal one. In particular, the actual Fe loading is considerably lower than the nominal one for the catalysts prepared from all cluster salts (Figure 5), whereas the gold content is almost as expected.

Figure 5. ICP Fe loading *vs*. nominal Fe content for titania catalysts prepared using, respectively, (▲)$[NEt_4][HFe_3(CO)_{11}]$; (♦)$[NEt_4][AuFe_4(CO)_{16}]$ and (■)$[NEt_4]_4[Au_4Fe_4(CO)_{16}]$ cluster salts.

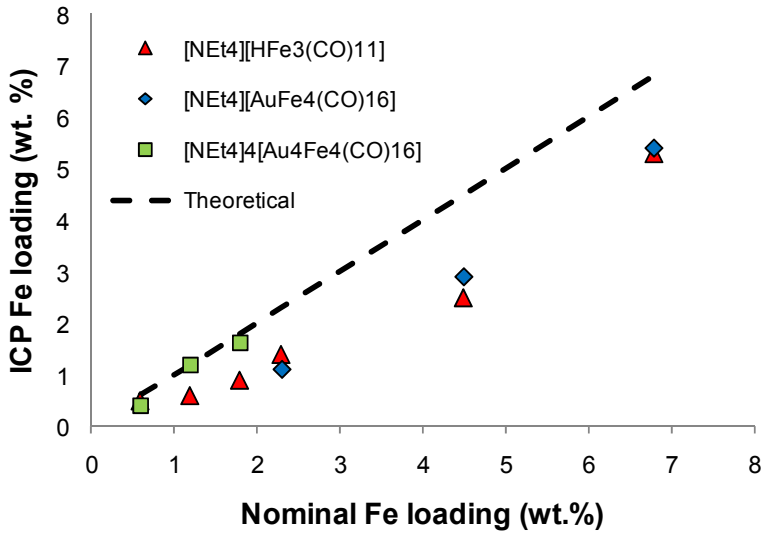

In all cases, this can be explained by assuming that iron is partially lost during the thermal treatment in the form of the volatile $Fe(CO)_5$, whereas gold is completely retained. This hypothesis is corroborated by the presence of an endothermic process at approx. 110 °C in the DSC diagram registered under nitrogen, in fair agreement with $Fe(CO)_5$ evaporation (b.p. 103 °C). Moreover, evolution of $Fe(CO)_5$

during thermal treatment of the as-prepared catalysts has been confirmed by condensation of the gases evolved in a cold trap and their consequent analyses by FT-IR.

With the aim of better controlling the bi-metallic cluster decomposition over the support, avoiding $Fe(CO)_5$ loss, a more detailed study was also carried out on catalyst pretreatment conditions.

In order to reduce the extent of Fe loss, the formation at low temperature of volatile $Fe(CO)_5$ compound should be prevented or at least minimized by using more suitable operative conditions. Thus, with the intention of avoiding the $Fe(CO)_5$ formation during cluster decomposition, a wet air flow was used in the course of $Fe_{2.3}Au_2$-Ce pretreatment at 100 °C, instead of dry air. In this way iron oxidation should occur simultaneously with cluster decomposition, being facilitated by the presence of water, avoiding the escape of $Fe(CO)_5$ from the support surface.

Some of this "as-prepared" sample ($Fe_{2.3}Au_2$-Ce-W sample) was characterized and tested without performing any other treatment in order to verify if the wet air pretreatment caused any change in the catalyst properties. Moreover, part of the $Fe_{2.3}Au_2$-Ce pretreated in wet air was also thermally treated at 400 °C under nitrogen ($Fe_{2.3}Au_2$-Ce-W-400) in order to compare its performances with the standard sample (Table 2).

Table 2. ICP results of $Fe_{2.3}Au_2$-Ce samples pretreated under different conditions.

Catalyst	Drying conditions	Thermal treatment conditions	Nominal Fe loading (wt.%)	Measured Fe loading (wt.%)
$Fe_{2.3}Au_2$-Ce-D	Air at 100 °C	-	2.3	1.9
$Fe_{2.3}Au_2$-Ce-D-400	Air at 100 °C	N_2 at 400 °C		1.6
$Fe_{2.3}Au_2$-Ce-W	Flowing Wet Air	-		2.3
$Fe_{2.3}Au_2$-Ce-W-400	Flowing Wet Air	N_2 at 400 °C		2.0

These data clearly indicate that iron loss is lower for samples pretreated in wet air, confirming the possibility of limiting the evolution of $Fe(CO)_5$ and consequently reducing the discrepancy between the theoretical and the real iron loading observed for samples treated in dry air.

Wet air pretreatment does not influence iron dispersion on ceria. Nevertheless, a detrimental effect on gold dispersion was observed (Table 3).

In fact, gold crystallites present on samples pretreated in wet-air are larger than the ones dispersed on samples pretreated in dry air. Moreover, the gold re-dispersion with high temperature observed for this latter system was absent in the material pretreated in wet air.

The worse gold dispersion observed with this last treatment may be related to the fast iron oxidation caused by water, which could lead to higher local temperature, responsible for gold sintering.

Table 3. Surface area and Au crystal size of $Fe_{2.3}Au_2$-Ce samples pretreated under different conditions.

Catalyst	Surface Area (m^2/g)	Au particle size (nm)
$Fe_{2.3}Au_2$-Ce-D	-	7.7
$Fe_{2.3}Au_2$-Ce-D-400	73	4.8
$Fe_{2.3}Au_2$-Ce-W	-	8.5
$Fe_{2.3}Au_2$-Ce-W-400	70	7.1

2.3. Characterization of Supported Gold/Iron Catalysts

Typical diffraction patterns of freshly prepared catalysts are shown in Figure 6. These analyses showed that the support phase (CeO_2 or TiO_2) is predominant; no detectable crystallite formation of any kind of ferric oxide or hydroxide was observed. For metallic Au, broad peaks were detected at about 38° and 44°.

Figure 6. XRD patterns of bimetallic titania (**a**) and ceria (**b**) catalysts prepared with $[NEt_4][AuFe_4(CO)_{16}]$.

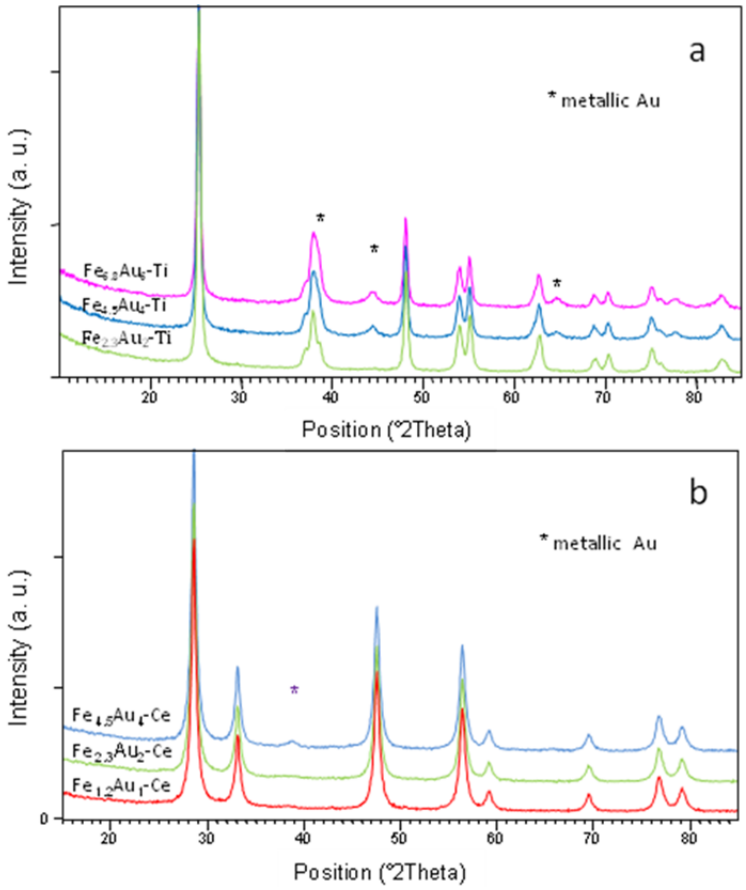

The average size of gold particles is given in Table 4. The corresponding size after catalytic operation is also shown in the same table. It is evident that the presence of an increasing amount of active phase leads to a slight increase of the average size of gold particles, but these results also indicate that the Au crystal growth can be reasonably controlled by utilizing the optimized thermal treatment conditions in N_2.

Table 4. Au particle size for fresh and spent Au-FeO_x-Ti and Au-FeO_x-Ce catalysts.

Catalyst	Au particle size Fresh (nm)	Au particle size Spent (nm)
$Fe_{0.6}Au_2$-Ti	6.0	6.0
$Fe_{1.2}Au_4$-Ti	6.6	6.7
$Fe_{1.8}Au_6$-Ti	7.4	7.6
$Fe_{2.3}Au_2$-Ti	<3.0	3.7
$Fe_{4.5}Au_4$-Ti	6.9	8.7

Table 4. *Cont.*

$Fe_{6.8}Au_6$-Ti	7.0	7.3
$Fe_{1.2}Au_1$-Ce	<3.0	3.0
$Fe_{2.3}Au_2$-Ce	4.8	5.0
$Fe_{4.5}Au_4$-Ce	9.0	9.1

Moreover, data regarding the degree of gold dispersion after catalytic operations showed only minor changes compared to the corresponding as-prepared samples, indicating a high stability of the prepared catalysts. Similar results have been obtained for FeO_x-supported systems with no detectable peaks related to crystallite of any kind of ferric oxides or hydroxide.

The dispersed Au/FeO_x particles on different support were studied by combining structural information from high-resolution TEM imaging and elemental mapping using high-angle annular dark-field scanning transmission electron microscopy (HAADF-STEM) and EDX. As an example, a clear image of gold nanoparticle over support is shown in Figure 7 with a HRTEM image obtained on $Fe_{2.3}Au_2$-Ce catalyst. Unfortunately, the presence of metallic iron or other iron oxides species on the catalysts could not be unambiguously identified on any of studied systems due to the fact that most of the reflections due to gold, ceria and iron crystals superimpose within the experimental precision achieved on the recorded diffraction patterns. However, with EDX mapping it was possible to observe the distribution of even the non-crystalline Fe species, which appeared to be uniformly dispersed all over the different supports [29,30]. Thus, as a general conclusion, TEM results were fairly in agreement with the findings of the XRD studies and suggest that iron oxide was well dispersed and not segregated either before or after the catalytic reaction. Moreover, the distribution of the gold particle dimensions, calculated from HAADF images, was also in good agreement with the average Au size estimated by XRD.

Figure 7. High Resolution TEM image of $Fe_{2.3}Au_2$-Ce sample.

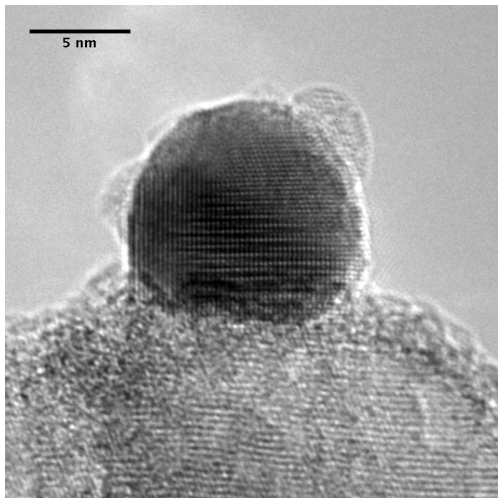

The surface content and the oxidation state of the catalysts were characterized by XPS before and after catalytic tests for all studied materials (Table 5); increasing the Au/support and Fe/support ratios may be correlated with the increased loading of these elements in the catalysts. However, the Au/Fe ratio was systematically below the bulk ratio determined by ICP. These results suggest that the atoms

of iron cover the atoms of gold. Indeed, in this kind of configuration, atoms of gold will be less available for XPS analyses and will thus take less part in the signal/spectra. Concerning the oxidation state of different elements, the binding energy of gold always corresponds to the metallic state (Au°). Moreover, the catalytic test does not seem to have an influence on the oxidation state of gold. The Fe $2p_{3/2}$ peak and the iron binding energy were similar in the presence and in the absence of gold in the catalyst. This peak exhibits a shoulder at about 710 eV and can be fitted with two peaks which, according to their binding energy, are attributed to Fe^{3+} (711 eV) and Fe^{2+} (709.8 eV) species [31]. Thus, the iron oxide layer appeared to be composed of a mixture of Fe_2O_3 and FeO or Fe_3O_4. According to the TPR data, the presence at the surface of some amount of iron hydroxide cannot be ruled out either.

Table 5. Atomic concentration ratios and binding energy of gold and iron in the catalysts.

Catalysts	Atomic concentration ratios		Binding Energy (eV)	
	Au/Fe XPS	Au/Fe ICP	Au 4f	Fe 2p
$Fe_{2.3}Au_2$-Ti	0.12	0.52	83.9	710.5
$Fe_{2.3}Au_2$-Ti-s	0.16	0.52	83.6	710.2
$Fe_{4.5}Au_4$-Ti	0.07	0.47	84.0	710.6
$Fe_{4.5}Au_4$-Ti-s	0.07	0.47	83.9	710.3
$Fe_{4.5}$-Ti	/	/	/	710.6
$Fe_{1.2}Au_1$-Ce	0.03	0.40	83.9	710.6
$Fe_{2.3}Au_2$-Ce	0.04	0.30	83.8	710.4
$Fe_{4.5}Au_4$-Ce	0.03	0.24	83.8	710.4

Temperature programmed reduction is a valuable technique in the understanding of the redox behavior of the catalysts. In scientific literature, a sizable effort has been devoted to the study of the reduction of unsupported and supported iron oxides [32]. Nevertheless, the nature of the total process is extremely complex and may vary with the physicochemical characteristics of the iron oxide or with the conditions of its reduction [33].

The reduction of the hydroxylated iron oxide species and that of hematite to Fe_3O_4 were observed for all FeO_x catalysts. Moreover, since the hydrogen consumed was found to be significantly greater than that necessary for the reduction [29,30], especially for catalysts at low iron content, it may be suggested that some reduction associated with the supports, whether TiO_2 or CeO_2, might overlap that of iron oxides. It is, in fact, known [34,35] that the presence of some metals can influence the reduction of oxygen species in TiO_2, and a strong interaction generally occurs between iron oxides and ceria [34,35].

The preparation of the catalysts by utilizing the gold/iron carbonyl cluster leads to the formation of species with very high reducibility. Such as an example we report in Figure 8 the comparison among H_2-TPR profile of support as is (CeO_2), monometallic $Fe_{1.2}$-Ce and $Fe_{1.2}Au_1$-Ce samples. In the case of bi-component ceria supported catalyst, gold presence increases iron reducibility and strongly influences CeO_2 reduction. In all reduction profiles obtained for bi-component samples, a peak appears at around 150 °C, confirming that gold/iron carbonyl cluster deposition on ceria leads to the formation of highly reducible iron and ceria species. TPR data reported in literature indicate that gold can cause a decrease in the strength of the surface Fe-O and Ce-O bonds adjacent to gold atoms, thus leading to a higher surface lattice oxygen mobility and therefore to a higher reactivity of these oxygens [6,36].

Figure 8. Comparison among H_2-TPR profile of (-) CeO_2, (-) $Fe_{1.2}$-Ce and (-) $Fe_{1.2}Au_1$-Ce samples.

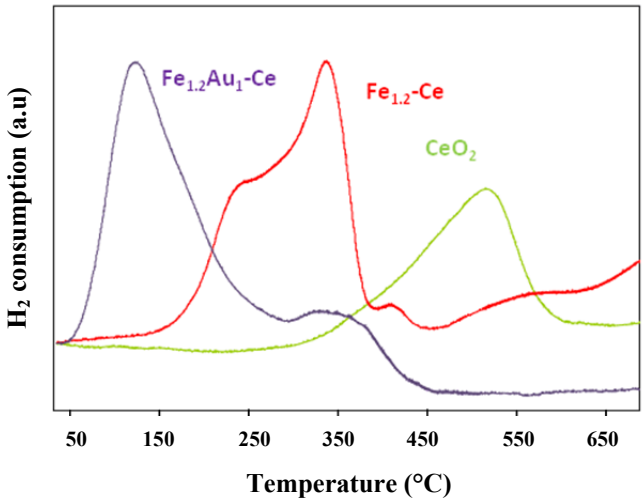

2.4. Catalysis by Supported Bimetallic Clusters

2.4.1. Toluene and Methanol Combustion

The catalytic performance of all samples was tested in the total combustion of toluene and methanol, chosen as representative molecules of VOC [29,30]. At this point, we must emphasize that the purpose of the catalytic measurements was to provide a criterion for ranking the activity of our materials with different organics rather than to demonstrate optimized catalytic performance in absolute terms.

The total oxidation of toluene was investigated over TiO_2 supported gold/iron catalysts. All the gold/iron cluster-derived catalysts exhibited an excellent stability under catalytic conditions in toluene total oxidation and the catalytic activity was demonstrated to depend on both the iron and the gold content. The presence of gold was demonstrated to enhance the selectivity of iron oxides towards the complete oxidation of toluene while the extent of the interaction between the two metals resulted important for catalytic activity [29].

Catalytic results obtained on FeO_x- and Au/FeO_x-ceria-supported catalysts have shown that the presence of iron species on the support does not significantly affect the total oxidation of methanol, whereas Au has a strong positive effect on the performances of catalysts toward this reaction, being the catalytic activity of the gold/iron oxide systems much higher than that of the bare ceria and FeO_x/CeO_2 catalysts [30]. The observed trend of activity appears to be in good agreement with H_2-TPR results obtained for these systems. In fact, the temperature at which 50% methanol conversion is reached has been found to be inversely related to the temperature of the maximum of the reduction peak for the $Au/FeO_x/CeO_2$ samples, as shown in Figure 9. Moreover, the greatest activity for methanol combustion, observed on the bi-component catalyst with the lowest metal loading ($Fe_{1.2}Au_1$-Ce sample) can also be correlated with the gold nanoparticles dimension. In fact, as it was reported in Table 4, $Fe_{1.2}Au_1$-Ce sample exhibits the smallest gold crystallite, confirming the assumption that oxygen mobility can be enhanced by oxygen vacancies in a close contact with small gold particles.

Figure 9. Temperature of 50% methanol conversion (■) and Tmax of the reduction peak (▲) in function of gold loading for $Au/FeO_x/CeO_2$ samples.

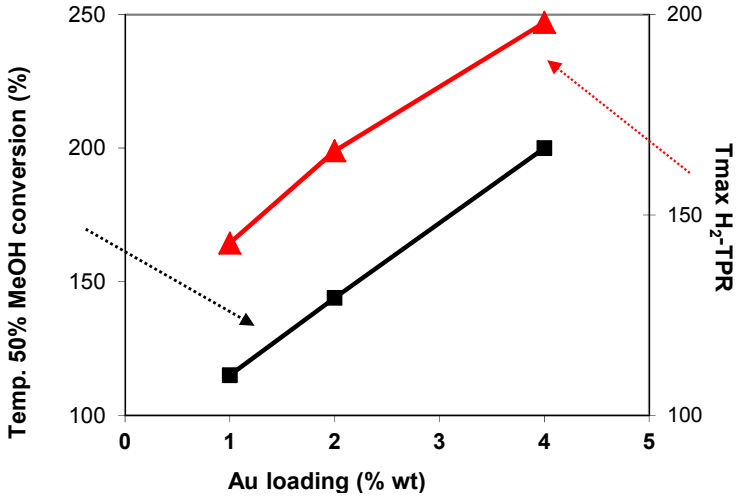

2.4.2. Catalytic Oxidation of CO in the Presence of H_2 (PROX)

Au/FeO_x-Ce catalysts were also tested in the PROX reaction; in fact, both iron oxide and ceria are considered suitable supports for CO oxidation gold catalysts. CO conversion curves obtained with these catalysts at different metal loadings are shown in Figure 10.

Figure 10. CO conversion as a function of reaction temperature over Au/FeO_x-Ce catalysts. Symbols: $Fe_{1.2}Au_1$-Ce (▲); $Fe_{2.3}Au_2$-Ce (■); $Fe_{4.5}Au_4$-Ce (×).

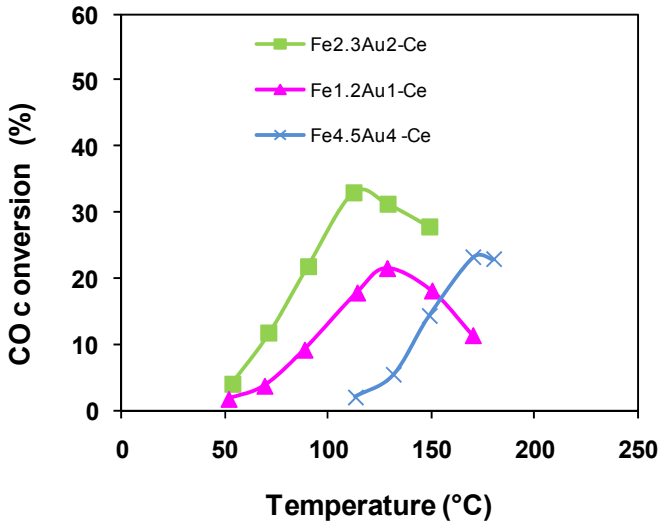

On all catalysts, CO conversion increased with rising temperature, reaching a maximum which was respectively around 20–25% for $Fe_{1.2}Au_1$-Ce and $Fe_{4.5}Au_4$-Ce, and 35% for $Fe_{2.3}Au_2$-Ce; the latter was found to be the most active sample among the bi-component ceria catalysts.

These data indicated that the CO oxidation activity of Au/FeO_x-Ce catalysts is strongly affected by metal loading on ceria, which influences metal dispersion and redox properties of the samples.

The catalytic activity in the PROX reaction observed for Au/FeO_x-Ce systems follows the order: $Fe_{2.3}Au_2$-Ce > $Fe_{1.2}Au_1$-Ce > $Fe_{4.5}Au_4$-Ce.

This trend can be justified in terms of catalyst metal dispersion: $Fe_{4.5}Au_4$-Ce showed the worst activity since the Au particle sizes are quite large for CO activation (9 nm).

The difference observed between the two samples with lower metal content may, instead, be explained in terms of the number of active sites: the $Fe_{2.3}Au_2$-Ce sample obviously contains more active sites than $Fe_{1.2}Au_1$-Ce, and Au average particle sizes are still suitable for CO oxidation, measuring less than 5 nm.

However, the CO oxidation activity observed for these samples is not really high compared with literature data. This is probably due to the very low Au/Fe surface ratio inferred from XPS data, which was found to be much lower than the bulk ratio. In fact, a kind of encapsulation effect of gold by iron and FeO_x atoms may be supposed, making the active sites less accessible for CO adsorption and activation. In this way, the positive effect that was expected to be achieved by iron addition to the Au-Ce system proved to be greatly reduced by this kind of disposition of the metal over the support. Generally, in fact, FeO_x species are responsible for providing the hydroxyl groups needed for the catalytic cycle, but also oxygen defect sites at which oxygen can chemisorb [16].

All these considerations become important, taking into account the fact that on Au/iron oxide catalysts, PROX reaction occurs through a Mars-van Krevelen mechanism, which entails active lattice oxygen species of the support reacting with CO adsorbed on gold particles and/or at the metal-support interface [37]. Actually, the effect of gold on the reducibility of oxide species on the catalyst surfaces was clearly observed in all Au/FeO_x-Ce catalyst reduction patterns, mainly for the samples with the lower metal content, on which higher CO oxidation was achieved.

The effect of the different thermal treatments performed on $Fe_{2.3}Au_2$-Ce (Table 1) on the catalytic activity in preferential CO oxidation was also investigated. The performances in the PROX reaction were found to be higher in the case of the samples treated at the highest temperatures, as shown in Figure 11. The observed trend in the CO oxidation activity for $Fe_{2.3}Au_2$-Ce material treated in different ways depends firstly on Au dispersion on the samples. In fact, Au crystal size is larger in the case of the dried catalyst (7.7 nm), which showed the lowest activity, while the sizes are almost the same in the two samples treated under nitrogen at 200 °C and 400 °C, respectively. Between these last two samples, even if the sample treated at 400 °C is more active at lower temperatures, a higher conversion can be achieved on $Fe_{2.3}Au_2$-D-200 (Figure 11b).

Figure 11. CO conversion (**a**) and CO maximum conversion (**b**) on $Fe_{2.3}Au_2$-Ce samples depending on thermal treatment temperature. Symbols: $Fe_{2.3}Au_2$-Ce-D (■); $Fe_{2.3}Au_2$-Ce-D-200 (▲), $Fe_{2.3}Au_2$-Ce-D-400 (×).

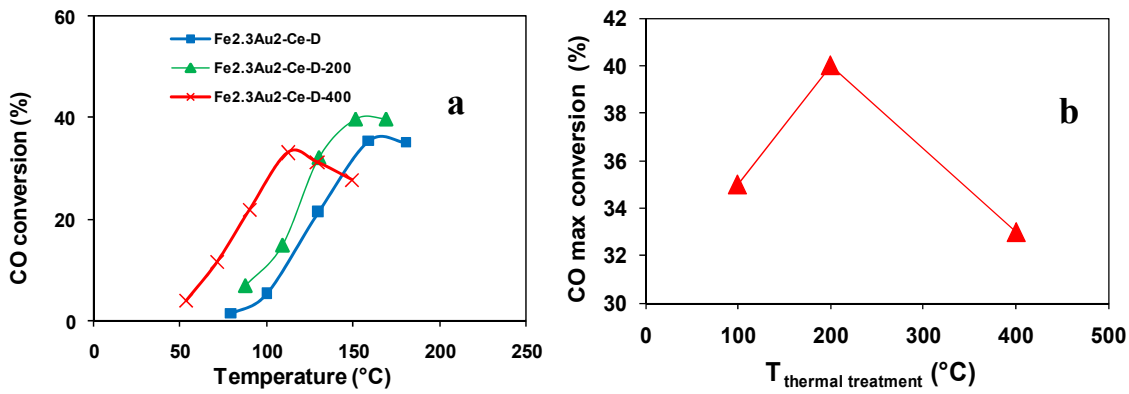

$Fe_{2.3}Au_2$-Ce catalysts treated at 200 °C were also found to be the most selective at temperatures over 120 °C. This behavior is in agreement with the data reported in literature [37]; even if the differences in the catalytic activity are not very great, they confirm the possibility of obtaining more hydroxylated iron oxide species, responsible for a higher CO oxidation activity, tuning the temperature used during catalyst thermal treatment.

CO oxidation activity on the $Fe_{2.3}Au_2$-Ce system was also found to be affected by the pre-treatment conditions (in dry or wet air—samples reported in Tables 2 and 3). Moreover, the thermal treatment at high temperature (400 °C in N_2) of these materials leads to catalysts with higher activity. In summary, concerning the influence of pre-treatment conditions on PROX results, the activity order observed was: $Fe_{2.3}Au_2$-Ce-D-400 > $Fe_{2.3}Au_2$-Ce-W-400 > $Fe_{2.3}Au_2$-Ce-W > $Fe_{2.3}Au_2$-Ce-D. This trend can be correlated to the gold particle size. In fact a relation exists between Au crystal size and the temperature at which the maximum CO conversion can be achieved on the corresponding catalyst (Figure 12).

Figure 12. Temperature of the maximum CO conversion *versus* Au crystal size. Catalysts: $Fe_{2.3}Au_2$-Ce materials treated under different conditions and temperature.

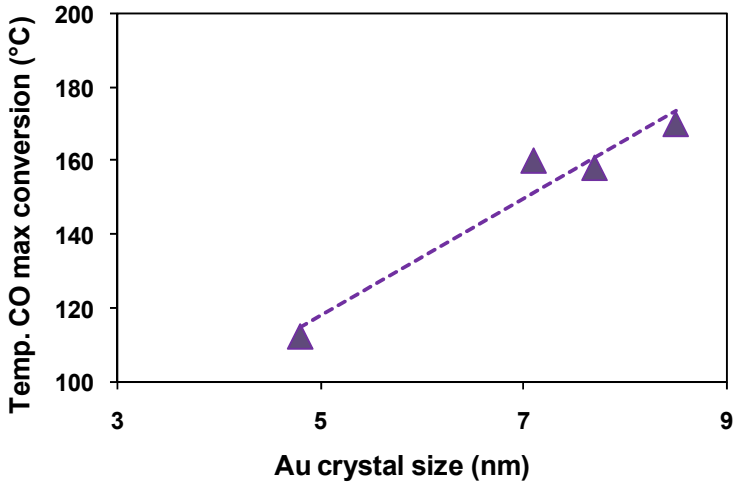

Sample $Fe_{2.3}Au_2$-Ce-D-400 was the most active catalyst at low temperature, having the smallest gold particle size, but its activity quickly decreased as the temperature raised. As a result, the lowest selectivity toward CO oxidation was achieved on this catalyst.

Figure 13a reports the selectivity towards the CO oxidation—expressed as CO_2 selectivity—and defined as the ratio of O_2 consumed for the CO oxidation respect to the total O_2 consumption, on catalysts treated under different conditions and temperature. The observed trends may be explained considering that CO mainly adsorbs on small Au particles and on the Au/oxide interface. Thus, in the presence of larger gold particles, CO activation is more difficult, depending on both Au dimensions and Au/oxide perimeter interface, the latter being shorter when gold dimensions increase [38].

In addition, it must be considered that when gold particles are larger, the oxygen supply, considered to enhance CO oxidation, was decreased, since a weaker oxygen mobility is achieved when interaction between Au and oxide species is not facilitated. In this way, CO oxidation occurs at higher temperatures and a higher CO_2 selectivity is obtained. The O_2 conversion trend obtained for this series of samples (Figure 13b) can also confirm these considerations: in fact, the lower oxygen conversion

observed on larger particles might also negatively affect the hydrogen oxidation, responsible for lowering CO oxidation.

Figure 13. Selectivity towards CO oxidation (**a**) and O_2 selectivity (**b**) on a $Fe_{2.3}Au_2$-Ce catalysts treated under different conditions.

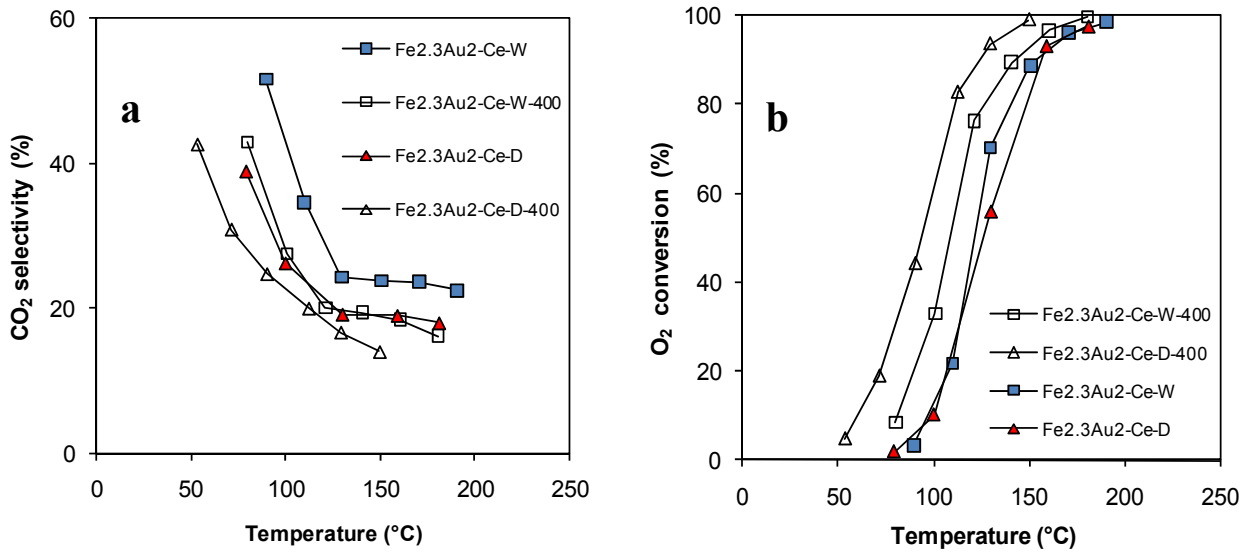

3. Experimental Section

3.1. Catalyst Preparation

Gold-iron catalysts with different Au and Fe contents were prepared by impregnation of the bimetallic carbonyl cluster salts $[NEt_4]_4[Au_4Fe_4(CO)_{16}]$ [39] and $[NEt_4][AuFe_4(CO)_{16}]$ [40] on commercial TiO_2 powder (Millennium Inorganic Chemicals powder DT51), CeO_2 powder (VP AdNano Ceria 90 Evonik), and mesoporous SBA-15 (prepared as indicated in [41]). In a typical experiment, the required amount of the carbonyl cluster was dissolved in degassed acetone (20–40 mL) under nitrogen and added dropwise over a period of 1 hour to an acetone suspension of the chosen support (10–15 g), previously degassed and stored under nitrogen. The resulting suspension was allowed to stir overnight, after which the solvent was removed in a vacuum at room temperature. If not differently indicated, the prepared samples were stored in air at ambient temperature, dried at 100 °C for 2 h in air, and thermal treated at 400 °C in flowing N_2. During this last treatment, the temperature was ramped at a rate of 10 °C/min from room temperature to 400 °C in nitrogen. The impregnation process was checked by FTIR in the ν(CO) region at different stages: starting cluster solution; acetone solution in contact with TiO_2; nujol mull of the dried powders before and after thermal treatment. For comparison, catalysts containing only Fe were prepared following a similar procedure by employing the homo-metallic $[NEt_4][HFe_3(CO)_{11}]$ cluster [42]. In this case the catalysts were dried at 100 °C for 2 h and calcined at 400 °C in air. Prepared samples will be indicated hereafter as Fe_x-S and Fe_xAu_y-S, where the numbers *x* and *y* refer to the theoretical iron and gold content in the materials and S indicates the support utilized (Ti = TiO_2; Ce = CeO_2 and SBA = SBA-15), *i.e.*, $Fe_{2.3}Au_2$-Ti indicates sample prepared with 2.3 wt.% iron and 2 wt.% gold supported on TiO_2.

3.2. Characterization of the Catalysts

Surface areas were measured by N_2 physisorption apparatus (Sorpty 1750 CE instruments) and single point BET analysis methods. Samples were pretreated under vacuum at 200 °C.

XRD measurements were carried out at room temperature with a Bragg/Brentano diffractometer (X'pertPro Panalytical) equipped with a fast X'Celerator detector, using Cu anode as X-ray source (Kα, λ = 1.5418 Å). For all samples the complete diffractogram was collected in the 2θ range 10–85°, counting 20 s each 0.05° step while a second acquisition was made for Au crystal size evaluation in the 2θ range 40–50°, counting 400 sec each 0.03 step. In fact, the coherent length of the Au crystalline domains was evaluated through single-line profile fitting of the reflection at 2θ 44.3°, since at this angle no overlap with the anatase pattern of the support was observed. Crystal size values were calculated from the widths at half maximum intensity using the Scherrer equation. IR spectra were recorded with a Perkin-Elmer SpectrumOne interferometer in CaF_2 cells. The reduction behavior of different samples was studied by means of Temperature Programmed Reduction using a Thermoquest TPDRO instrument under 5% H_2/Ar flow (20 mL min^{-1}). The temperature was raised from 60° to 700 °C with a heating rate of 10 °C min^{-1}.

XPS analyses were performed on a Kratos Axis Ultra spectrometer (Kratos Analytical: Manchester, UK) equipped with a monochromatized aluminium X-ray source (powered at 10 mA and 15 kV). The pressure in the analysis chamber was about 10–6 Pa. The analyzed area was 700 μm × 300 μm. The pass energy was set at 160 eV for the wide scan and 40 eV for narrow scans. Charge stabilization was achieved by using the Kratos Axis device. The following sequence of spectra was recorded: survey spectrum, C 1s, O 1s, Au 4f, Fe 2p, Ti 2p, and again C1s to check for charge stability as a function of time and the absence of degradation of the sample during the analyses. The C-(C, H) component of the C1s peak of carbon was fixed to 284.8 eV to set the binding energy scale. Molar fractions [%] were calculated using peak areas normalized on the basis of acquisition parameters after a linear background subtraction, experimental sensitivity factors, and transmission factors provided by the manufacturer. Spectra were decomposed with the CasaXPS program (Casa Software Ltd., Manchester, UK) with a Gaussian/Lorentzian (70:30) product function.

The real metal content on the catalysts was determined by ICP-AES analysis with a Fision 3410 + instrument.

Transmission Electron Microscopy (TEM) observations were carried out with a Fei Tecnai F20 TEM with a Schottky emitter and operating at 200 keV. The instrument is equipped with a Fischione High Angle Annular Dark Field Detector (HAADF) for Scanning Transmission Electron Microscopy (STEM) observations and with an Edax EDS PV9761N SUTW Energy Dispersive X-Ray Spectrometer (EDX) for X-rays microanalysis. The samples were ground in a mortar and treated with ultrasound in isopropyl alcohol to reduce the grain dimensions to a minimum. A droplet of the resulting finely dispersed suspension was evaporated at room temperature and atmospheric pressure on a copper grid with a holey carbon film for the analyses.

3.3. Catalytic Activity of Supported Clusters for Toluene and Methanol

Catalytic experiments with toluene and methanol were carried out in a fixed bed glass reactor at atmospheric pressure [29,30]. A K-type thermocouple was placed into the catalyst bed to monitor the reaction temperature. Each run used approximately 350 mg of catalyst in the form of 30–60 mesh (250–595 μm) particles, diluted with an inert powder of similar size for better temperature control. The total volumetric flow through the catalyst bed was held constant at 140 mL min^{-1}, 10 vol.% oxygen, 90 vol.% nitrogen and 1400 ppm of toluene or 2600 ppm of methanol. Analyses of reactants and products were carried out as follows: the products in the outlet stream were scrubbed in cold acetone maintained at −25°C by a F32 Julabo Thermostat. Analysis of reactants and products were carried out with a GC Clarus 500 (Perkin Elmer) equipped with a Elite FFAP column (30 m × 0.32 mm) and a FID. CO and CO_2 formed were separated on a capillary column Elite Plot Q (30 m × 0.32 mm), attached to a methanizer and analyzed with a flame ionization detector (FID). Particular care was devoted to the determination of the C balance, which was found to always fall between 95 and 105% (calculated as the comparison between converted toluene and the sum of the product yields).

3.4. Catalytic Activity of Supported Clusters for PROX Reaction

Catalytic activity tests were carried out in the gas phase at atmospheric pressure in a continuous-flow microreactor filled with catalyst (0.015–0.05 g, 80–140 mesh) diluted with an inert glass powder [43]. The gas composition (total flow rate: 80 mL/min) was 1% of CO and 1% of O_2, the rest being H_2. Before activity tests, catalysts were reduced in H_2 at 200 °C. The effluent gases were analyzed by an online gas chromatograph with a packed column (Carboxen1000) and a TCD. The selectivity towards CO oxidation was defined as the ratio of O_2 consumption for the CO oxidation to CO_2 respect to the total O_2 consumption.

4. Conclusions

Au/FeO_x and FeO_x catalysts supported on titania and ceria were prepared by impregnation of carbonyl clusters as precursors of highly dispersed active phase. Au/FeO_x were obtained by employing bi-metallic carbonyl cluster salts $[NEt_4]_4[Au_4Fe_4(CO)_{16}]$ (Fe/Au = 1) and $[NEt_4][AuFe_4(CO)_{16}]$ (Fe/Au = 4), while FeO_x samples were prepared by employing the homometallic $[NEt_4][HFe_3(CO)_{11}]$ cluster. Particular attention was taken in the optimization of a suitable thermal treatment in order to achieve, along with a good Au and Fe metal dispersion, the formation of appropriate species with good catalytic properties. The preparation method used for the synthesis of CeO_2- and TiO_2-supported materials resulted in small gold metallic nanoparticles surrounded by highly dispersed iron oxide species, essentially in an amorphous phase. Starting from both $[NEt_4]_4[Au_4Fe_4(CO)_{16}]$ and $[NEt_4][AuFe_4(CO)_{16}]$ salts, a very similar metal dispersion can be achieved either on ceria or on titania. Accordingly, the use of different metal oxides as supports does not seem to influence Au and Fe dispersion on the surface, probably due the fact that the active phase dispersion was mainly controlled by the rate of cluster decomposition at air. The results described herein confirmed that FeO_x species can stabilize small Au particles. In fact, keeping the gold content constant but introducing a higher iron amount by means of $[NEt_4][AuFe_4(CO)_{16}]$ salts gave a higher gold dispersion than using a

$[NEt_4]_4[Au_4Fe_4(CO)_{16}]$ cluster did. A kind of encapsulation of gold atoms by iron oxide species was obtained, since the Au/Fe surface ratio was found to be much lower than the bulk ratio.

A strong interaction between gold and oxide species was observed, both for iron oxide and the supports, especially for the ceria species, denoted by a significantly enhanced reducibility.

All prepared catalysts were tested in the total oxidation of VOCs, using toluene and methanol as probe molecules for aromatic and alcohol compounds, and in the PROX reaction. On both TiO_2- and CeO_2-supported catalysts, the introduction of gold, and consequently the higher oxygen mobility due to the weakening of both Fe-O and Ce-O bonds, leads to improved methanol combustion. Moreover, the catalytic activity was found to follow the same trend observed for catalyst reducibility.

Regarding PROX reaction it was verified that titania-based catalysts are less active than ceria ones, due to the lower reducibility of titania compared to ceria. In fact, the availability of lattice oxygen involved in CO total oxidation is much higher in the latter material.

However, the CO conversions observed for these samples are relatively low with respect to literature data. These scant results are probably due to the very low Au/Fe surface ratio inferred from XPS data. CO preferential oxidation was found to be strongly dependent on Au particle size, but also on the reducibility of surface oxygen, influenced by the different species which can be formed.

Actually, the effect of gold on the reducibility of oxide species present on the catalyst surface was clearly observed in all Au/FeO_x-Ce catalysts, especially for samples with lower metal content, on which higher CO conversion was achieved.

In spite of the non-optimized catalytic performance, this novel preparation method, employing carbonyl bi-component Fe-Au clusters with a well defined structure, resulted in well dispersed gold nanoparticles anchored to the support via an iron layer. In this way a good stabilization of gold particles was achieved, obtaining at the same time the beneficial effect of gold on iron oxide reducibility. These results indicate the possibility for this preparation method to find further applications for obtaining a good Au dispersion over supports on which the stabilization of gold nanoparticles is difficult. A first attempt on Au/FeO_x-supported SBA-15 mesoporous silica prepared by bi-metallic carbonyl cluster impregnation has been made, and some preliminary promising results have been obtained [40]. Nevertheless, a careful optimization of thermal treatment in the presence of steam, in order to improve Au dispersion and simultaneously favor the presence of more active iron species, is still necessary.

Acknowledgments

We thank the University of Bologna (Project CLUSTERCAT) for funding. Support by European Community, through the Network of Excellence IDECAT (Integrated Design of Catalytic Nanomaterials for a Sustainable Production) is also acknowledged. The authors are indebted for valuable discussion to Salvatore Scirè, Eric Gaigneaux and Cristina Femoni. Paolo Riccobene (University of Catania) is acknowledged for PROX investigation and Romain Delaigle (Université Catholique de Louvain) is acknowledged for XPS measurements.

References

1. Haruta, M. Catalysis of gold nanoparticles deposited on metal oxides. *CATTECH* **2002**, *6*, 102–115.
2. Hashmi, A.S.K.; Hutchings, G.J. Gold catalysis. *Angew. Chem. Int. Ed.* **2006**, *45*, 7896–7936.
3. Centeno, M.A; Paulis, M.; Montes, M.; Odriozola, J.A. Catalytic combustion of volatile organic compounds on gold/titanium oxynitride catalysts. *Appl. Catal. B* **2005**, *61*, 177–183.
4. Lakshmanan, P.; Delannoy, L.; Richard, V.; Méthivier, C.; Potvin, C.; Louis, C. Total oxidation of propene over $Au/xCeO_2$-Al_2O_3 catalysts: Influence of the CeO_2 loading and the activation treatment *Appl. Catal. B* **2010**, *94*, 117–124.
5. Minicò, S.; Scirè, S.; Crisafulli, C.; Galvagno, S. Influence of catalyst pretreatments on volatile organic compounds oxidation over gold/iron oxide. *Appl. Catal. B* **2001**, *34*, 277–285.
6. Minicò, S.; Scirè, S.; Crisafulli, C.; Maggiore, R.; Galvagno, S. Catalytic combustion of volatile organic compounds on gold/iron oxide catalysts. *Appl. Catal. B* **2000**, *28*, 245–251.
7. Laguna, O.H.; Romero-Sarria, F.; Centeno, M.A.; Odriozola, J.A. Gold supported on metal-doped ceria catalysts (M = Zr, Zn and Fe) for the preferential oxidation of CO (PROX). *J. Catal.* **2010**, *276*, 360–370.
8. Guczi, L. Bimetallic nano-particles: Featuring structure and reactivity. *Catal. Today* **2005**, *101*, 53–64.
9. Bordes, E. Synergistic effects in selective oxidation catalysis: Does phase cooperation result in site isolation? *Top. Catal.* **2001**, *15*, 131–137.
10. Alexeev, O.S.; Gates, B.C. Supported bimetallic cluster catalysts. *Ind. Eng. Chem. Res.* **2003**, *42*, 1571–1587.
11. Edwards, J.K.; Solsona, B.E.; Landon, P.; Carley, A.F.; Herzing, A.; Kiely, C.J.; Hutchings, G.J. Direct synthesis of hydrogen peroxide from H_2 and O_2 using TiO_2-supported Au-Pd catalysts. *J. Catal.* **2005**, *236*, 69–79.
12. Bianchi, C.L.; Canton, P.; Dimitratos, N.; Porta, F.; Prati, L. Selective oxidation of glycerol with oxygen using mono and bimetallic catalysts based on Au, Pd and Pt metals. *Catal. Today* **2005**, *102–103*, 203–212.
13. Venezia, A.M.; La Parola, V.; Deganello, G.; Pawelec, B.; Fierro, J.L.G. Synergetic effect of gold in Au/Pd catalysts during hydrodesulfurization reactions of model compounds. *J. Catal.* **2003**, *215*, 317–325.
14. Pasini, T.; Piccinini, M.; Blosi, M.; Bonelli, R.; Albonetti, S.; Dimitratos, N.; Lopez-Sanchez, J.A.; Sankar, M.; He, Q.; Kiely, C.J.; *et al.* Selective oxidation of 5-hydroxymethyl-2-furfural using supported gold-copper nanoparticles. *Green Chem.* **2011**, *13*, 2091–2099.
15. Carrettin, S.; Hao, Y.; Aguilar-Guerrero, V.; Gates, B.C.; Trasobares, S.; Calvino, J.; Corma, A. Increasing the number of oxygen vacancies on TiO_2 by doping with iron increases the activity of supported gold for CO oxidation *Chem. Eur. J.* **2007**, *13*, 7771–7779.
16. Moreau, F.; Bond, G.C. Preservation of the activity of supported gold catalysts for CO oxidation. *Top. Catal.* **2007**, *44*, 95–101.
17. Gluhoi, A.C.; Bogdanchikova, N.; Nieuwenhuys, B.E. The effect of different types of additives on the catalytic activity of Au/Al_2O_3 in propene total oxidation: Transition metal oxides and ceria. *J. Catal.* **2005**, *229*, 154–162.

18. Penkova, A.; Chakarova, K.; Laguna, O.H.; Hadjiivanov, K.; Romero-Sarria, F.; Centeno, M.A.; Odriozola, J.A. Redox chemistry of gold in a $Au/FeO_x/CeO_2$ CO oxidation catalyst *Catal. Commun.* **2009**, *10*, 1196–1202.
19. Laguna, O.H.; Centeno, M.A.; Arzamendi, G.; Gandia, L.M.; Romero-Sarria, F.; Odriozola, J.A. Iron-modified ceria and Au/ceria catalysts for total and preferential oxidation of CO (TOX and PROX). *Catal. Today* **2010**, *157*, 155–159.
20. Siani, A.; Captain, B.; Adams, R.D.; Alexeev, O.S.; Amiridis, M.D. Synthesis and Structural Characterization of SiO_2-Supported PtFe Catalysts Prepared from $PtFe_2(C_8H_{12})(CO)_8$. *Top. Catal.* **2011**, *54*, 318–333.
21. Schay, Z.; Lázár, K.; Mink, J.; Guczi, L. Spectroscopic and catalytic studies on metal carbonyl clusters supported on Cab-O-Sil. II. Impregnation and decomposition of $Ru_3(CO)_{12}$ and the mixture of $Ru_3(CO)_{12}$ and $Fe_3(CO)_{12}$. *J. Catal.* **1984**, *87*, 179–195.
22. Guczi L.; Beck A. Elementary steps in the formation of bimetallic catalysts derived from carbonyl clusters. *Polyhedron* **1988**, *22–23*, 2387–2392.
23. Guczi, L.; Beck, A.; Dobos, S. Metal clusters: A model for a molecular surface switch in the genesis of highly dispersed metal particles. *J. Mol. Catal.* **1992**, *74*, 317–322.
24. Femoni, C.; Kaswalder, F.; Iapalucci, M.C.; Longoni, G.; Zacchini, S. The possible role of metal carbonyl clusters in nanoscience and nanotechnologies. *Coord. Chem. Rev.* **2006**, *250*, 1580–1604.
25. Femoni, C.; Iapalucci, M.C.; Longoni, G.; Tiozzo, C.; Zacchini, S. An organometallic approach to gold nanoparticles: Synthesis and X-ray structure of CO-protected $Au_{21}Fe_{10}$, $Au_{22}Fe_{12}$, $Au_{28}Fe_{14}$, and $Au_{34}Fe_{14}$ clusters. *Angew. Chem. Int. Ed.* **2008**, *47*, 6666–6669.
26. Lopez-Acevedo, O.; Rintala, J.; Virtanen, S.; Femoni, C.; Tiozzo, C.; Grönbeck, H.; Pettersson, M.; Häkkinen, H. Characterization of iron-carbonyl-protected gold clusters. *J. Am. Chem. Soc.* **2009**, *131*, 12573–12575.
27. Femoni, C.; Iapalucci, M.C.; Longoni, G.; Tiozzo, C.; Wolowska, J.; Zacchini, S.; Zazzaroni, E. New hybrid semiconductor materials based on viologen salts of bimetallic Fe-Pt and Fe-Au carbonyl clusters: First structural characterization of the diradical π-dimer of the diethyl viologen monocation and EPR evidence of its triplet state. *Chem. Eur. J.* **2007**, *13*, 6544–6554.
28. Albonetti, S.; Bonelli, R.; Epoupa Mengou, J.; Femoni, C.; Tiozzo, C.; Zacchini, S.; Trifirò F. Gold/Iron carbonyl clusters as precursors for TiO_2 supported catalysts. *Catal. Today* **2008**, *137*, 483–488.
29. Albonetti, S.; Bonelli, R.; Delaigle, R.; Femoni, C.; Gaigneaux, E.M.; Morandi, V.; Orlandi, L.; Tiozzo, C.; Zacchini, S.; Trifirò, F. Catalytic combustion of toluene over cluster-derived gold/iron catalysts. *Appl. Catal. A* **2010**, *372*, 138–146.
30. Albonetti, S.; Bonelli, R.; Morandi, V.; Ortolani, L.; Riccobene, P.M.; Scirè, S.; Zacchini, S. Design of nano-sized FeO_x and Au/FeO_x catalysts supported on CeO_2 for total oxidation of VOC. *Appl. Catal. A* **2011**, *395*, 10–18.
31. Guczi, L.; Frey, K.; Beck, A.; Peto, G.; Daroczi, C.S.; Kruse, N.; Chnakin, S. Iron oxide overlayers on $Au/SiO_2/Si(1\ 0\ 0)$: Promoting effect of Au on the catalytic activity of iron oxide in CO oxidation. *Appl. Catal. A* **2005**, *291*, 116–125.
32. Munteanu, G.; Ilieva, L.; Andreeva, D. Kinetic parameters obtained from TPR data for α-Fe_2O_3 and Au/α-Fe_2O_3 systems. *Thermochim. Acta* **1997**, *291*, 171–177.

33. Jozwiak, W.K.; Kaczmarek, E.; Maniecki, T.P.; Ignaczak, W.; Maniukiewicz, W. Reduction behavior of iron oxides in hydrogen and carbon monoxide atmospheres. *Appl. Catal. A* **2007**, *326*, 17–27.
34. Li, K.Z.; Wang, H.; Wey, Y.G. Selective oxidation of carbon using iron-modified cerium oxide. *J. Phys. Chem. C* **2009**, *113*, 15288–15297.
35. Kaneko, H.; Miura, T.; Ishihara, H.; Taku, S.; Yokoyama, T.; Nakajima, H.; Tamaura, Y. Reactive ceramics of CeO_2-MO_x (M = Mn, Fe, Ni, Cu) for H_2 generation by two-step water splitting using concentrated solar thermal energy. *Energy* **2007**, *32*, 656–663.
36. Scirè, S.; Minicò, S.; Crisafulli, C.; Satriano, C.; Pistone, A. Catalytic combustion of volatile organic compounds on gold/cerium oxide catalyst. *Appl. Catal. B* **2003**, *40*, 43–49.
37. Scirè, S.; Crisafulli, C.; Minicò, S.; Condorelli, G.; di Mauro, G.A. Selective oxidation of CO in H_2-rich stream over gold/iron oxide: An insight on the effect of catalyst pretreatment. *J. Mol. Catal. A* **2008**, *284*, 24–32.
38. Guczi, L.; Beck, A.; Frey, K. Role of promoting oxide morphology dictating the activity of Au/SiO2 catalyst in CO oxidation. *Gold Bull.* **2009**, *42*, 5–12.
39. Albano, V.G.; Calderoni, F.; Iapalucci, M.C.; Longoni, G.; Monari, M. Synthesis of $[AuFe_2(CO)_8]^{3-}$ and $[Au_4Fe_4(CO)_{16}]^{4-}$: X-ray structure of the $[Au_4Fe_4(CO)_{16}]^{4-}$ cluster anion in its $[NEt_4]^+$ salt. *J. Chem. Soc. Chem. Commun*. **1995**, *4*, 433–434.
40. Albano, V.G.; Aureli, R.; Iapalucci, M.C.; Laschi, F.; Longoni, G.; Monari, M.; Zanello, P. Synthesis, characterization and electrochemical behaviour of the $[Fe_4Au(CO)_{16}]^{n-}$ (n = 1,2,3) clusters. X ray structure of $[NMe_3CH_2Ph][Fe_4Au(CO)_{16}]Cl$. *J. Chem. Soc. Chem. Commun*. **1993**, *19*, 1501–1502.
41. Bonelli, R.; Lucarelli, C.; Pasini, T.; Liotta, L.F.; Zacchini, S.; Albonetti, S. Total oxidation of volatile organic compounds on Au/FeO_x catalysts supported on mesoporous SBA-15 silica. *Appl. Catal. A* **2011**, *400*, 54–60.
42. Farmery, K.; Kilner, M.; Greatrex, R.; Greenwood, N.N. Structural studies of the carbonylate and carbonyl hydride anions of iron. *J. Chem. Soc. A* **1969**, 2339–2345.
43. Albonetti, S.; Bonelli, R.; Delaigle, R.; Gaigneaux, E.M.; Femoni, C.; Riccobene, P.M.; Scirè, S.; Tiozzo, C.; Zacchini, S.; Trifirò, F. Design of nano-sized FeO_x and Au/FeO_x supported catalysts for total oxidation of VOC and preferential oxidation of CO. *Stud. Surf. Sci. Catal.* **2010**, *175*, 786–788.